Published online: July 25, 2016

Scientific Report

TRANSPARENT PROCESS

EMBO reports

Structural role of the T94I rhodopsin mutation in congenital stationary night blindness

Ankita Singhal[1], Ying Guo[2], Milos Matkovic[1], Gebhard Schertler[1,3], Xavier Deupi[1,4], Elsa CY Yan[2] & Joerg Standfuss[1,*]

Abstract

Congenital stationary night blindness (CSNB) is an inherited and non-progressive retinal dysfunction. Here, we present the crystal structure of CSNB-causing T94I$^{2.61}$ rhodopsin in the active conformation at 2.3 Å resolution. The introduced hydrophobic side chain prolongs the lifetime of the G protein activating metarhodopsin-II state by establishing a direct van der Waals contact with K296$^{7.43}$, the site of retinal attachment. This is in stark contrast to the light-activated state of the CSNB-causing G90D$^{2.57}$ mutation, where the charged mutation forms a salt bridge with K296$^{7.43}$. To find the common denominator between these two functional modifications, we combined our structural data with a kinetic biochemical analysis and molecular dynamics simulations. Our results indicate that both the charged G90D$^{2.57}$ and the hydrophobic T94I$^{2.61}$ mutation alter the dark state by weakening the interaction between the Schiff base (SB) and its counterion E113$^{3.28}$. We propose that this interference with the tight regulation of the dim light photoreceptor rhodopsin increases background noise in the visual system and causes the loss of night vision characteristic for CSNB patients.

Keywords congenital stationary night blindness; constitutive activity; G protein-coupled receptors; rhodopsin; visual system

Subject Categories Membrane & Intracellular Transport; Molecular Biology of Disease; Structural Biology

DOI 10.15252/embr.201642671 | Received 4 May 2016 | Revised 5 July 2016 | Accepted 7 July 2016 | Published online 25 July 2016

EMBO Reports (2016) 17: 1431–1440

Introduction

G protein-coupled receptors (GPCRs) are a large class of membrane proteins responsible for signal transduction in response to a variety of external signals such as small chemicals and peptides, and sensory stimuli like taste and odor molecules or light. However, GPCRs also transduce signals in the absence of external inputs, a phenomenon known as "constitutive activity". In addition, constitutive activity can also be caused by point mutations that disturb the inactive conformation of the receptor and/or stabilize its active state. Constitutively active point mutations have been characterized in many GPCRs and commonly translate into a pathological outcome [1].

The visual photoreceptor rhodopsin is a highly sensitive and finely tuned GPCR with a minimal level of constitutive (or "dark") activity. Specifically, the rate of spontaneous activation events in primate rod cells has been estimated to be 5.2×10^{-11} per second, corresponding to a half-life of the inactive state of 420 years [2]. This exceptionally low level of basal activity is attributable to the covalently bound ligand 11-*cis* retinal, which acts as inverse agonist that further decreases activity below that of the apoprotein opsin, which itself is 10^6-fold less active than the active metarhodopsin-II state with covalently bound agonist all-*trans* retinal [3].

Any increase in the level of the dark activity of rhodopsin reduces the signal-to-noise ratio affecting the light-sensing capability of the rod cells. Thus, constitutive activity in rhodopsin has been discussed as the cause of diseases (for a recent review [4]), such as retinitis pigmentosa (RP) [5,6] or congenital stationary night blindness (CSNB) [7,8]. RP is a progressive form of blindness that severely impairs the visual field, whereas CSNB is a much milder and often precursor form affecting only dim light vision. In CSNB patients [9–12] and mouse models of the disease [13–15], the rhodopsin-containing rod cells are functionally desensitized as if under constant activation at low gain. This increased dark activity has been suggested to result from a faster rate of thermal isomerization [9], the presence of constitutively active opsin [7] or of a pre-activated dark state [14], or simply a reduction in the amount of photoexcitable pigment [15]. Understanding the fundamental causes of these processes is key to unraveling the molecular mechanism of CSNB.

In a previous work, we presented the crystal structure of the CSNB-causing G90D$^{2.57}$ (superscript denotes Ballesteros Weinstein numbering) rhodopsin mutant [16]. This structure visualized how the mutated aspartate in TM2 forms a salt bridge with residue K296$^{7.43}$ in TM7, impairing the formation of the Schiff base (SB) that, under normal conditions, connects retinal to the protein. Here

1 Division of Biology and Chemistry, Laboratory of Biomolecular Research, Paul Scherrer Institute, Villigen, Switzerland
2 Department of Chemistry, Yale University, New Haven, CT, USA
3 Deparment of Biology, ETH Zurich, Zürich, Switzerland
4 Condensed Matter Theory Group, Paul Scherrer Institute, Villigen, Switzerland
*Corresponding author. Tel: +41 56 310 2586; E-mail: joerg.standfuss@psi.ch

we present a study of the T94I$^{2.61}$ rhodopsin mutant, which exhibits the same disease phenotype as G90D$^{2.57}$ [11]. However, while the T94I$^{2.61}$ mutation is close to G90D$^{2.57}$, the different physicochemical properties of the mutated residue side chains must translate into a different molecular cause for the disease phenotype. In order to elucidate this cause, we have solved the crystal structure of the T94I$^{2.61}$ mutant in the metarhodopsin-II active conformation. Structural comparison of G90D$^{2.57}$ and T94I$^{2.61}$ rhodopsin in combination with molecular dynamics simulations and a kinetic analysis of their dark states advance our understanding of the molecular causes of CSNB and its differences to the progressing RP phenotype.

Results and Discussion

Structural comparison of CSNB mutants in the active state

In a first step, we crystallized light-activated T94I$^{2.61}$ rhodopsin in the presence and absence of the C-terminal peptidic end of the G protein alpha subunit (GαCT2 peptide) [17]. Two active conformation structures were determined at 2.8 and 2.3 Å resolution (Table EV1). As in our previous rhodopsin crystallization projects, all constructs used in this study also contain an additional thermostabilizing disulfide bridge, depicted as (c-c), to enhance the stability [18] and crystallizability [19] without changing the rhodopsin activation pathway [20].

Overall T94I$^{2.61}$ rhodopsin adopts the conformation of metarhodopsin-II obtained by soaking opsin crystals with all-*trans* retinal (rmsd of α atoms = 0.353) [17] and compares well to constitutively active M257Y metarhodopsin-II (rmsd of α atoms = 0.35) [21] and the overall fold of the CSNB mutant G90D$^{2.57}$ (rmsd of α atoms = 0.29) [16].

However, the effect of the T94I$^{2.61}$ mutation on the retinal binding pocket is strikingly different to that of G90D$^{2.57}$ (Fig 1). The G90D$^{2.57}$ mutation introduces an aspartic acid that interferes with the covalent binding of all-*trans* retinal by forming a salt bridge with K296$^{7.43}$, resulting in the stabilization of an active conformation. T94$^{2.61}$ is positioned only one helix turn away from G90$^{2.57}$, also pointing toward the retinal SB (Fig EV1). Thus, we initially assumed that the introduction of the bulky hydrophobic amino acid isoleucine at this position would perturb retinal binding similarly to the G90D$^{2.57}$ mutant. However, the methyl group of I94$^{2.61}$ and the Cε atom of K296$^{7.43}$ are at a van der Waals contact distance, but this does not result into retinal hydrolysis (compare middle and right lower panels in Fig 1). Thus, the T94I$^{2.61}$ mutation yields a "clean" metarhodopsin-II conformation with covalently bound all-*trans* retinal.

The T94I$^{2.61}$ mutation does not result into major structural changes in the retinal binding pocket, yet replacement of the native hydrophilic Thr for the hydrophobic Ile modifies the physicochemical properties of this region. We suggest that this alteration, in turn, affects the process of rhodopsin deactivation as follows. The deactivation process requires the hydrolytic cleavage of the SB in the metarhodopsin-II state to allow the release of all-*trans* retinal and the subsequent regeneration of the pigment with 11-*cis* retinal. SB hydrolysis is initiated by a base-catalyzed water molecule and proceeds through a protonated carbinolamine intermediate [22]. A water-mediated hydrogen bond network in the retinal binding pocket is critical for SB stability and determines the rate of this hydrolysis step [23–25]. T94I$^{2.61}$ is one of the few known mutations that increase the rate of SB hydrolysis in the rhodopsin dark state but decrease it in metarhodopsin-II [8]. Our 2.3 Å crystal structure of this mutant reveals the water network around retinal in an unprecedented detail: We observe four new water molecules that are probably not specific for this mutant, as the structure of the retinal binding pocket has not changed compared to previous structures of metarhodopsin-II [17,21]. However, one of the previously described water molecules in this region is missing in our structure, likely because the hydrophobic mutation T94I$^{2.61}$ eliminates the hydrogen-bonding potential at this position. In wild-type metarhodopsin-II [17], this water mediates an interaction between T94$^{2.61}$ and the retinal counterion E113$^{3.28}$. We speculate that this missing water in the T94I$^{2.61}$ mutant alters the first step of the SB hydrolysis by affecting the formation of the carbinolamine intermediate. In order to further envisage the influence of the bulkier hydrophobic I94$^{2.61}$ side chain on the retinal hydrolysis mechanism, we compared the accessibility surface area of the SB in T94I$^{2.61}$ and wild-type metarhodopsin-II. We found that the mutation results in a 30% decrease in the accessibility of Cε and Nζ of K296$^{7.43}$ that can be attributed to the van der Waals interaction of these atoms with I94$^{2.61}$. Thus, it seems likely that the I94$^{2.61}$ side chain sterically hinders the access to the SB or directly alters the formation of the tetrahedral protonated carbinolamine intermediate during SB hydrolysis.

In summary, we suggest that the impairment of the hydrogen bond network in the vicinity of the retinal SB as well as steric hindrance in the hydrolysis reaction is responsible for the increased lifetime of metarhodopsin-II observed in T94I$^{2.61}$ rhodopsin. This hypothesis is in agreement with the faster kinetics of retinal release in metarhodopsin-II for the T94A$^{2.61}$ mutant compared to T94I$^{2.61}$ [26], as the smaller alanine side chain would not be able to affect retinal hydrolysis as described above.

Effect of CSNB mutants on stability of the rhodopsin dark state

To investigate the impact of CSNB-inducing mutations on overall protein integrity, we first measured rhodopsin stability using a fluorescence-based thermal-shift assay. The stability of the T94I$^{2.61}$ rhodopsin mutant was compared to the thermostabilized wild type, both in the presence and absence of the 11-*cis* and all-*trans* retinal isomers (Fig EV2). Interestingly, upon addition of 11-*cis* retinal, the transition melting temperature of T94I$^{2.61}$ rhodopsin increased only from 49 to 53°C, whereas the effect on WT rhodopsin was much more pronounced, with a shift of the transition temperature from 53 to 63°C. We have observed a similar destabilizing effect of the G90D$^{2.57}$ mutation on the rhodopsin dark state [16]. However, in contrast to G90D$^{2.57}$, the T94I$^{2.61}$ mutation does not increase the stability of the opsin state, presumably because the introduced isoleucine is unable to form a stabilizing salt bridge interaction with K296$^{7.43}$. These thermal-shift measurements indicate an overall lower stability of the dark state for the two CSNB mutations compared to the WT.

We investigated whether this effect is specifically due to disturbance of SB integrity by measuring the rate of thermal decay as a function of the decrease in absorption from retinal with protonated SB (Fig 2A–D). We determined decay times of 797 ± 25 min, 22.2 ± 1.3 min, and 424 ± 31 min for WT, T94I$^{2.61}$, and G90D$^{2.57}$,

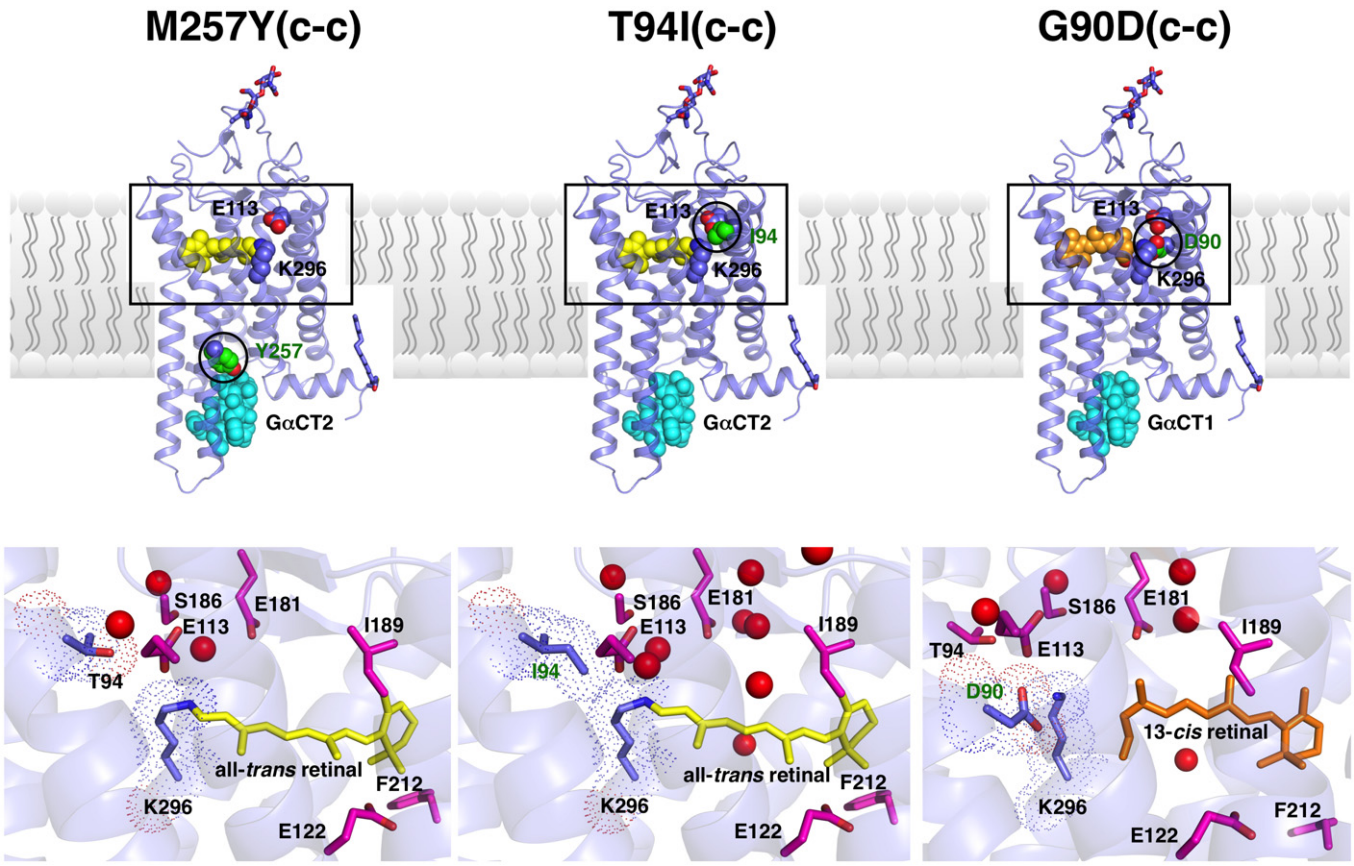

Figure 1. Comparison of constitutively active rhodopsin mutants M257Y$^{6.40}$ (left [21]), T94I$^{2.61}$ (middle), and G90D$^{2.57}$ (right [16]).
All-*trans* (yellow) and *cis* retinal isomers (orange); the side of retinal attachment K296$^{7.43}$ (blue slate); the retinal counterion E113$^{3.28}$ (blue slate); GαCT peptides (cyan); and the constitutively activating mutations M257Y$^{6.40}$, T94I$^{2.61}$, and G90D$^{2.57}$ (green) are shown as spheres. Palmitoylation at C323^{H8} and glycosylation at N15^{NT} are shown as sticks. The lower panels compare the M257Y$^{6.40}$, T94I$^{2.61}$, and G90D$^{2.57}$ retinal binding pockets. All constructs also contain an additional thermostabilizing disulfide bridge, depicted as (c-c), to enhance the stability [18] and crystallizability [19] without changing the rhodopsin activation pathway [20].

respectively. The faster rate of thermal decay in both mutants indicates that the retinal binding pocket in the vicinity of the retinal SB is altered. According to our data, the T94I$^{2.61}$ dark state decays 35 times faster than the WT, whereas G90D$^{2.57}$ decays only 2 times faster than the WT suggesting that the T94I$^{2.61}$ dark state is less stable.

Decay of the dark state involves two simultaneous spontaneous processes, that is, thermal isomerization of 11-*cis* to all-*trans* retinal and SB hydrolysis [27,28]. We measured the rate of thermal isomerization by HPLC analysis after extracting retinal after various times of incubation at 55°C (Fig 2E–H). The decrease in the 11-*cis* retinal peak coincides with increase in the all-*trans* retinal peak, validating the thermal isomerization of retinal. In addition, some minor peaks of 13-*cis*-15-*syn* and 11-*cis*-15-*anti* also appeared. The fraction of 11-*cis* retinal, which was the major peak at the beginning for all mutants, was plotted as a function of time. Fitting to a single exponential decay yielded a decay time of 1,136 ± 27 min for WT, 58.6 ± 6.4 min for T94I$^{2.61}$, and 503 ± 93 min for G90D$^{2.57}$; that is, the decay by thermal isomerization of retinal in T94I$^{2.61}$ and G90D$^{2.57}$ is 19 and 2 time faster, respectively, than the WT. Similarly, the kinetics of SB hydrolysis were measured by acid denaturation of the dark state (Fig 2I–L). Hydrochloric acid was used to reduce the pH to 1–2, causing the denaturation of the protein. At the beginning of the experiment (t = 0), the dominant peak was at 440 nm, corresponding to the protonated species, which was gradually subdued by an increase in the 380 nm peak due to appearance of free retinal. The decrease in the 440 nm peak was plotted as a function of time as a single exponential decay curve, yielding a decay rate of 797 ± 25 min for WT, 22.2 ± 1.3 min for T94I$^{2.61}$, and 406 ± 91 min for G90D$^{2.57}$. These data, showing that SB hydrolysis in T94I$^{2.61}$ is 35 times faster than in WT, also confirm the lower stability of the T94I$^{2.61}$ dark state. This rate of retinal hydrolysis is significantly faster than the twofold rate increase observed for G90D$^{2.57}$ rhodopsin. In summary, both CSNB mutations increase the rates of thermal decay, retinal thermal isomerization and of SB hydrolysis, although to different extents.

Structural impact of CSNB mutations on the rhodopsin dark state

Our X-ray crystallographic data provide interesting insights at the molecular level into the effect of CSNB mutations on the rhodopsin active metarhodopsin-II state. However, despite extensive efforts, we were not able to crystallize the dark state of either G90D$^{2.57}$ or T94I$^{2.61}$. This is likely a consequence of conformational

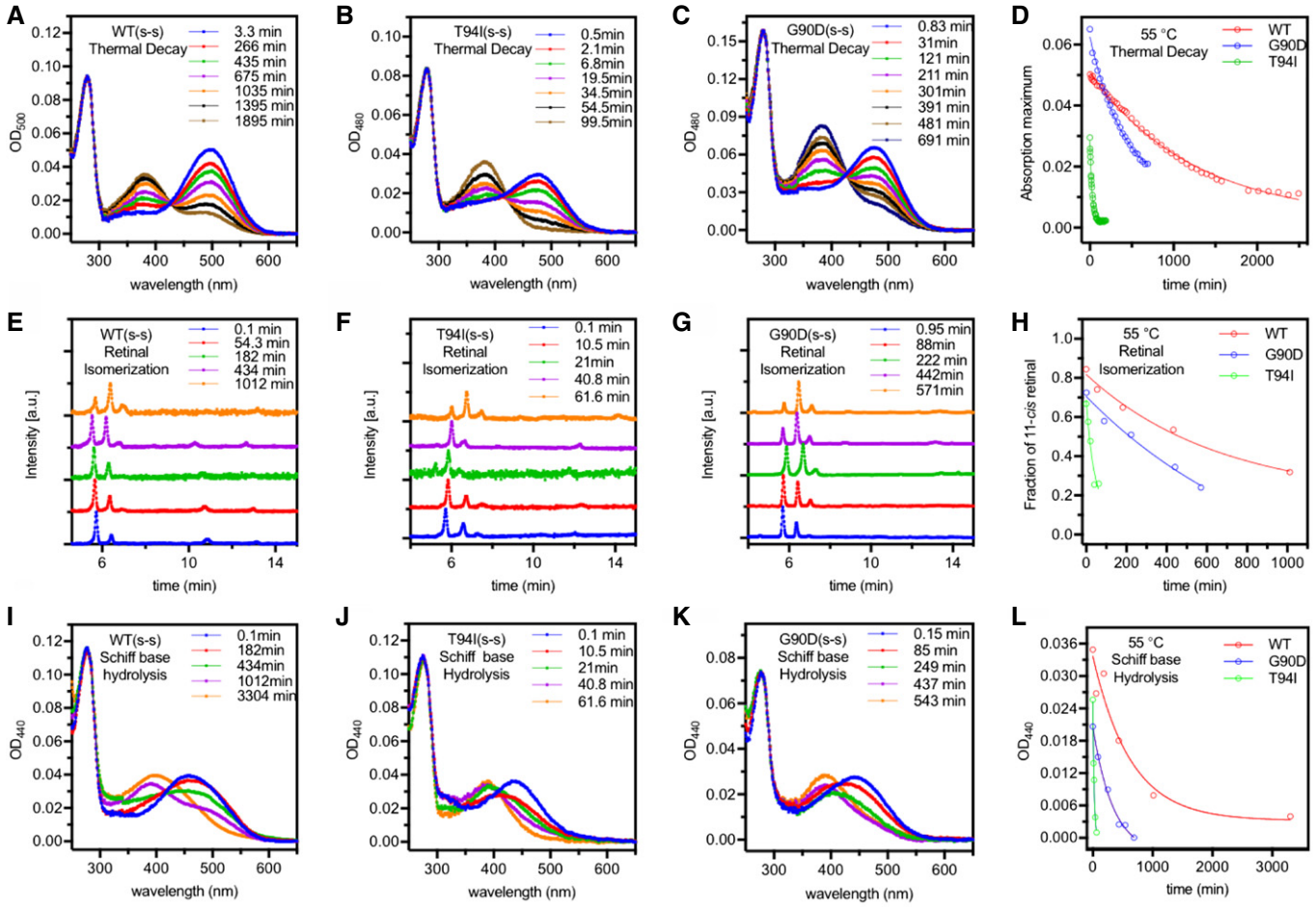

Figure 2. Kinetic characterization of the rhodopsin dark state.

A–C Thermal decay of dark state rhodopsin: WT (A), T94I (B), and G90D (C) rhodopsin. The spectra are normalized to the OD_{280} and OD_{500}/OD_{480} at $t = 0$.

D Absorption maximum plotted as a function of time and fitted to a single exponential decay.

E–G Retinal isomerization in the rhodopsin dark state: WT (E), T94I (F), and G90D (G) rhodopsin.

H The fraction of 11-*cis* retinal is plotted as a function of time and fitted to a single exponential decay.

I–K SB stability in dark state rhodopsin: WT (I), T94I (J), and G90D (K) rhodopsin.

L OD_{440} is plotted as a function of time and fitted to a single exponential decay.

Data information: All decay rates were measured at 55°C.

heterogeneity in agreement with our biochemical analysis (see above) and with prior studies showing increased hydroxylamine reactivity [29], structural rearrangements [30], and lower stability [31] in the G90D$^{2.57}$ dark state.

But what is the cause of this conformational heterogeneity? The exceptional stability (and low basal activity) of the rhodopsin dark state arises from the covalent binding of the 11-*cis* retinal inverse agonist to the protein by means of a protonated SB. A rigid hydrogen-bonding network [23] and additional ionic interactions between the protonated SB and the counterion E113$^{3.28}$ [32,33] are also crucial to stabilize the rhodopsin dark state. Photoisomerization to all-*trans* retinal results in deprotonation of the SB and concomitant opening of the salt bridge with E113$^{3.28}$. Triggering this "primary switch" is one of the hallmarks of rhodopsin activation. Interestingly, all four known CSNB mutations (G90D, T94I, A292E, A295V) are in close proximity to the E113$^{3.28}$-SB pair, and it has been shown before that both the G90D$^{2.57}$ [7,34] and T94I$^{2.61}$ mutations [8,35] do interfere with the E113$^{3.28}$ counterion. Therefore, the influence of the CSNB mutations on the SB-E113$^{3.28}$ pair is a likely candidate as the source of conformational instability of the dark state.

As we cannot assess the impact of the G90D$^{2.57}$ and T94I$^{2.61}$ mutations on the dark state of rhodopsin by X-ray crystallography, we have studied these systems using molecular dynamics simulations. In the reference system WT(c-c) rhodopsin, the ligand binding pocket (defined as all residues having atoms within 6 Å of the retinal) remained remarkably stable, with a final root mean square deviation (rmsd) of 1.2 Å^2 and a distance between the protonated SB and the counterion of 1.9 Å (Fig 3). Simulation of G90D$^{2.57}$ rhodopsin resulted in a slightly higher overall rmsd of 1.9 Å, yet led in contrast to the WT, to a significant rearrangement of the binding pocket. The side chain of G90D$^{2.57}$ moves in between the SB and the

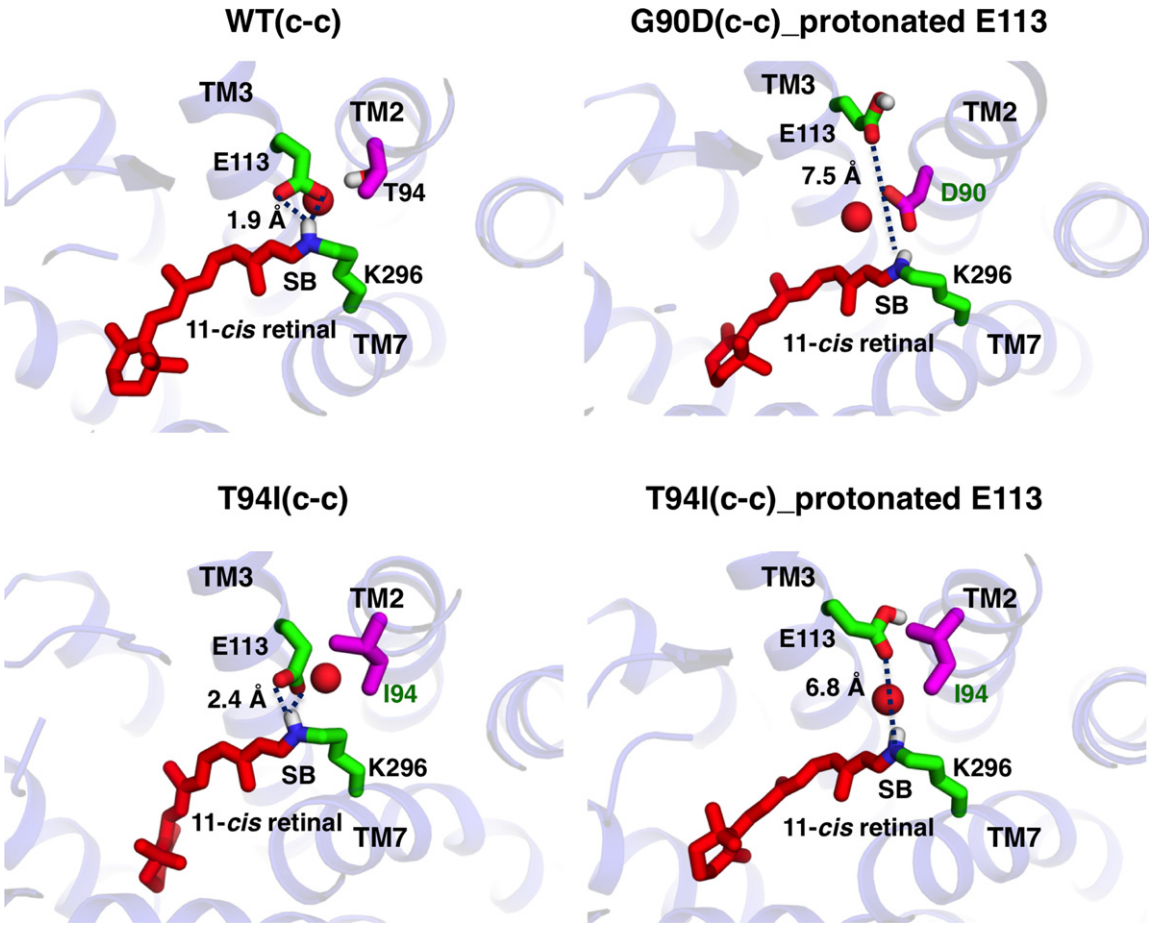

Figure 3. Accelerated molecular dynamic simulation of the rhodopsin dark state: WT, G90D$^{2.57}$, T94I$^{2.61}$, and T94I$^{2.61}$ with protonated E113$^{3.28}$.
In the absence of the G90D$^{2.57}$ and T94I$^{2.61}$ dark state structure, both aspartate and isoleucine were placed in the WT (1GZM [48]) using a favorable rotamer without introducing major clashes with the rest of the protein. However, both isoleucine and aspartate in the dark state structures introduced clashes with several amino acids and were therefore optimized using energy minimization before simulation. WT simulation was done with the protonated SB while in the G90D$^{2.57}$ system, both E113$^{3.28}$ and SB were protonated [36]. The protonated state of E113$^{3.28}$ was unknown in T94I$^{2.61}$; therefore, simulation was done for both deprotonated and protonated E113$^{3.28}$. The T94I$^{2.61}$ dark state conformation with deprotonated E113$^{3.28}$ was similar to that of the WT and was stable, whereas the dark state of G90D$^{2.57}$ and T94I$^{2.61}$ with protonated E113$^{3.28}$ was unstable with a concomitant movement of E113$^{3.28}$ residue away from the SB, thereby causing movement of TM3 and opening of the E113$^{3.28}$-SB activation switch. In contrast to the crystal structures, the orientation of the retinal β-ionone ring in the simulations was variable with respect to the polyene chain. This indicates a degree of positional freedom within the hydrophobic binding pocket.

counterion E113$^{3.28}$, and, as a result, the distance between E113$^{3.28}$ and the SB increased to 7.5 Å, resembling an opening of the primary activation switch (Movie EV1).

The protonation state of the E113$^{3.28}$ residue in the T94I$^{2.61}$ dark state is unknown, and therefore, we simulated the T94I$^{2.61}$ dark state with either a deprotonated E113$^{3.28}$, as in WT rhodopsin, or a protonated E113$^{3.28}$, as in the CSNB mutant G90D$^{2.57}$ [36]. In the first case, we only observed a partial opening (2.4 Å) of the E113$^{3.28}$-SB activation switch and a noticeable expansion of the binding pocket. On the other hand, in the simulation with protonated E113$^{3.28}$, the T94I$^{2.61}$ side chain moved in between SB and E113$^{3.28}$ in a similar position as observed in the simulation of the G90D$^{2.57}$ mutant. In this case, the distance between E113$^{3.28}$ and the SB increased to 6.8 Å, also resembling the opening of the activation switch.

Thus, by combining our biochemical and spectroscopy data with molecular dynamics simulations, we suggest that both T94I$^{2.61}$ and G90D$^{2.57}$ CSNB mutants are able to destabilize the dark state specifically by weakening the primary activation switch mediated by the counterion E113$^{3.28}$.

Relevance to CSNB

In this study, we used crystallographic, biochemical, and computational methods to find the common denominator for the CSNB-causing rhodopsin mutations G90D$^{2.57}$ and T94I$^{2.61}$. While it is yet unknown whether G90D$^{2.57}$ and T94I$^{2.61}$ cause CSNB by the same mechanism, there are several indications that they at least share some common features. First of all, although the mutated residues have very different physico-chemical properties, they are located on adjacent helix turns and form part of the retinal binding pocket. Furthermore, both mutations result in similar phenotypes: Patients have a normal amount of rhodopsin in the retina and structurally preserved rods, despite massive loss of rod function and impaired dim light vision on standard clinical tests [9,11,12]. In

mouse models of CSNB, the rhodopsin-carrying rod cells are desensitized as under continuous activation at low gain [13,14]. These aberrant signals compete with dim external stimuli and reduce night vision (Fig 4).

It seems clear that the source of this basal activity is the mutant rhodopsin, but it is less clear which precise molecular state (i.e. light-activated, opsin, or dark state) is the ultimate responsible. G90D$^{2.57}$ displaces the retinal counterion E113$^{3.28}$ in the dark state [7] and can form a salt bridge with K296$^{7.43}$ to stabilize an active opsin conformation with mixed retinal isomers [16]. On the other hand, T94I$^{2.61}$ results in a "clean" metarhodopsin-II with covalently bound all-*trans* retinal. Moreover, both mutations have opposite biochemical effects on the metarhodopsin-II state; light-activated G90D$^{2.57}$ decays quickly, while the lifetime of T94I$^{2.61}$ metarhodopsin-II increases, in agreement with previous reports [8]. Overall, these results suggest that the effects on the light-activated receptor are not the common denominator of the two CSNB mutations.

Another potential source of the increased basal activity in rods is the active state of the apoprotein opsin [7]. It is generally assumed that opsin exists in equilibrium between an active and inactive conformation [37]. While all four known CSNB mutations have been shown to be constitutively active and thus increase the fraction of active opsin [12], this effect is small in the case of T94I$^{2.61}$ [8]. According to a study of mutations in the retinal entry channel [26], T94I$^{2.61}$ may even reduce constitutive activity of opsin. The same study shows increased constitutive activity for 11 out of 15 mutations close to the retinal binding pocket, none of which is correlated with CSNB. An important mechanism to suppress any remaining opsin constitutive activity in rod cells is phosphorylation by GRK1 and successive binding of arrestin-1. Therefore, disturbing this mechanism might contribute to the increased background activity characteristic for CSNB. However, while G90D$^{2.57}$ opsin does bind arrestin-1 less efficiently, T94I$^{2.61}$ does it as well as wild type [38]. Overall, our data suggest that the opsin form can be excluded as common denominator between the two CSNB mutations.

In vivo studies with transgenic mice carrying the G90D$^{2.57}$ gene show another convincing argument for excluding the constitutively active opsin species as main cause of CSNB. The transgenic mice have a similar disease phenotype as CSNB patients, in the sense that they have light adapted rod cells and decreased light sensitivity. In contrast to previous studies done on COS cells [7] and transgenic frogs [39], the G90D$^{2.57}$ mutation did not show increased basal activity of opsin in mice [14]. Furthermore, the effects of the mutants could not be reversed by regeneration with 11-*cis* retinal as would have been expected as it completely suppresses the remaining constitutive activity of opsin. In agreement with the findings in transgenic mice, desensitization in

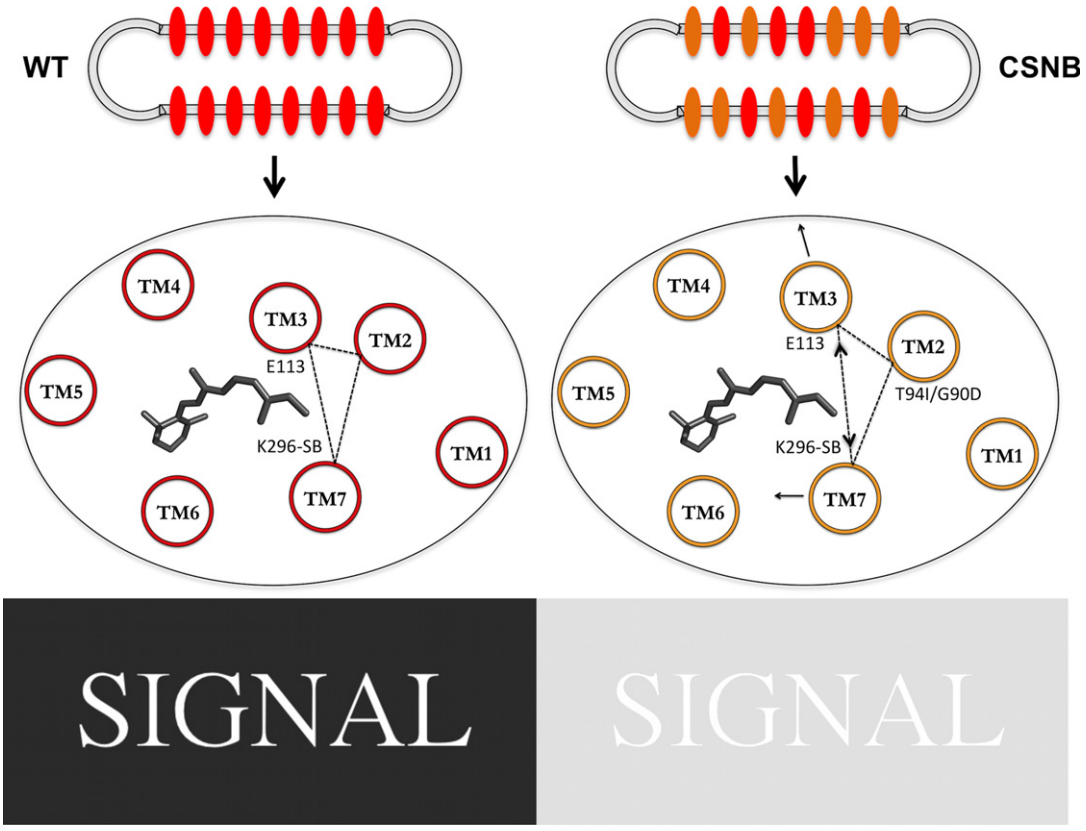

Figure 4. The molecular cause of congenital stationary night blindness (CSNB).
Disk membranes (upper panels) in the rod cells of healthy individuals (left) and CSNB patients (right) contain a normal distribution of rhodopsin. Interference of the T94I$^{2.61}$ and G90D$^{2.57}$ mutations with the E113$^{3.28}$-SB activation switch (middle panels) leads to partial activation of a small portion of rhodopsins (orange). The resulting basal stimulation of the visual system leads to a decreased signal-to-noise ratio (lower panel) and impaired night vision in affected patients.

G90D$^{2.57}$ patients is not reversed even after 12 h of dark adaptation [13]. The authors suggest that the disease is caused by a disturbed rhodopsin dark state that activates the visual cascade with a low gain. Indeed, we observe that the dark states of G90D$^{2.57}$ and T94I$^{2.61}$ share many features indicative of a disturbed inactive conformation. Our data show that both mutants have a significantly reduced thermal stability, increased rates of SB hydrolysis and of retinal isomerization, and blue-shifted absorption maxima compatible with a partially protonated counterion. These results indicate that the alterations are close to the protonated SB, and our MD simulations allow us to hypothesize that both mutations can open the E113$^{3.28}$-SB activation switch. This activation switch together with an extended hydrogen-bonding network and covalent binding of the 11-*cis* retinal inverse agonist are key determinants suppressing the basal activity of rhodopsin.

Decreasing the strength of the E113$^{3.28}$-SB activation switch is not sufficient to fully activate rhodopsin. For this, at least one additional requirement is needed, the uptake of a proton by E134$^{3.49}$ of the conserved E(D)RY motif at the cytoplasmic terminus of TM3 [40]. Without this, second protonation switch activity should be very low, and indeed, both the G90D$^{2.57}$ and T94I$^{2.61}$ dark states do not have increased basal activity within the detection limit of *in vitro* G protein activation assays [7,8]. However, human rod cells are highly optimized for single photon sensitivity, and a small increase in activity (i.e., constitutive activation of only a small fraction of the approximately 10^8 rhodopsin molecules in a rod cell), which would be hard to detect in *in vitro* assays, should be sufficient to reduce dim light vision leading to CSNB.

In summary, we provide a comprehensive analysis of the structural, dynamic, and biochemical properties of two mutations that, despite their different chemical nature, are causing the same hereditary form of night blindness. Our data provide a structural basis to understand CSNB. It further provides clues to unravel the molecular basis of rhodopsin mediated RP, which results in a similar impaired vision under dim light, but in addition is associated with progressive degeneration of rods. Structures of other constitutively active rhodopsin class GPCRs may tell us to what extent similar disease mechanisms are found outside the visual system.

Materials and Methods

Crystallographic sample preparation and crystal refinement

Purification and crystallization of recombinant rhodopsin were carried out as described [16,41]. Data were collected using the high-resolution diffractometer setup of beamlines PXI-X06SA and PXIII-X06DA at the Swiss Light Source (SLS) following a low-dose/high-redundancy data collection strategy. Data were integrated and scaled using XDS [42]. Phases were obtained by molecular replacement using the program PHASER [43] and the polypeptide of M257Y rhodopsin (pdb code: 4a4m [21]) as search model. The resulting solution was refined using iterative cycles of model building in COOT [44] and refinement (rigid body, energy minimization, simulated annealing, individual B-factor refinement) with the PHENIX program suite [45].

Thermal-shift assay

Thermal-shift assays were performed in a carry Eclipse fluorimeter (Varian) equipped with multisample holder. Thermal denaturation was followed using the thiol-specific maleimide fluorochrome CPM (N-[4-(7-diethylamino-4-methyl-3-coumarinyl)phenyl]maleimide) as described [16,46]. Conditions were as follows: 5 μg of rhodopsin purified by 1D4 immunoaffinity purification was diluted into 120 μl ice-cold buffer (100 mM NaCl, 10 mM Hepes pH 7.5, and 0.125% DM). Immediately before the measurement CPM (3 mg/ml in DMSO) was diluted 1:30 into buffer and 10 μl of this mixture added to the reaction mix. The above-mentioned steps were repeated with opsin with supplementation of either 10 μM 11-*cis* or all-*trans*-retinal and incubated in the dark for 2 h. WT(c-c) was taken as the control. An excitation wavelength of 387 nm and an emission wavelength of 463 nm were used for measurements of opsin. To minimize spectral overlap, an excitation wavelength of 420 nm was used for measurements in the presence of 11-*cis* and all-*trans* retinal. During each thermal denaturation experiment, the temperature was increased from 20 to 90°C at 2°C/min. The resulting melting curve was fitted using a sigmoidal boltzmann equation to obtain TM_{50} values. Average TM_{50} values and standard deviations were obtained from four measurements.

Sample purification for biochemical and kinetic analysis

Cell pellets were detergent solubilized in 50 mM Tris, 100 mM NaCl, 1 mM $CaCl_2$, 1% w/v DDM, 0.1 mM PMSF, pH 6.8 for 3 h at 4°C. After solubilization, membrane fragments were centrifuged and regenerated with excess 11-*cis* retinal (7.15 μM) for 2 h at 4°C. Rhodopsin was purified using the 1D4 antibody coupled to Sepharose beads. The beads were washed three times with 50 mM Tris, 100 mM NaCl, 0.1% DDM, pH 6.8, and three times with 50 mM sodium phosphate, 0.1% DDM, pH 6.5 (Buffer A). The rhodopsin samples were eluted in Buffer A containing 1D4 peptide for competitive binding to the antibody (final concentration of 1D4 peptide in elution buffer is 0.18 mg/ml).

UV-visible spectroscopy and thermal decay

Thermal decay of dark state rhodopsin was monitored by UV-visible spectroscopy. Buffer A (~2 ml) was equilibrated in a water-jacketed cuvette at 55°C. The temperature was confirmed using a thermal couple. At $t = 0$, ice-cold, concentrated rhodopsin solution (~20 μl) was added to the buffer equilibrated at 55°C to give a final concentration of 1–3 μM. Since the volume of the concentrated rhodopsin sample is small compared to the volume of buffer A, the temperature change upon the addition of sample could be neglected. Previously, we did a control experiment by monitoring the temperature change after adding the sample into the buffer, the temperature change was compensated within 5 s. UV-visible spectra were recorded over time with Shimadzu UV-2450 spectrophotometer.

HPLC analysis

Retinal was extracted from the samples as described in Liu *et al* [47]. Briefly, the samples were incubated on ice for

30 min with hydroxylamine (pH 7) to break the SB linkage between retinal and the opsin protein. Methanol, dichloromethane, and hexane were added to denature opsin and extract the retinaloximes. The isomeric mixture of retinaloximes was analyzed by HPLC (Beckman Coulter SYSTEM GOLD® 125 Solvent Module) on a silica column (Beckman Coulter Ultrasphere 4.6 × 250 mm) and a mobile phase of hexane supplemented with 8% diethyl ether and 0.33% ethanol. Absorbance at 360 nm was used for detection (Beckman Coulter SYSTEM GOLD® 168 Detector).

Molecular dynamics simulations

For the simulations of the dark state of wild-type rhodopsin, we used as a starting conformation the structure of bovine rhodopsin in a trigonal crystal form (1GZM [48]). The dark state of the rhodopsin mutants G90D$^{2.57}$ and T94I$^{2.61}$ was modeled using the 1GZM structure with additional stabilizing disulfide bond [18] as a template, and substituting residue G90 or T94 to Asp or Ile using the backbone-dependent rotamer library implemented in PyMOL (The PyMOL Molecular Graphics System, Version 1.2r3pre, Schrödinger, LLC), and choosing the Asp and Ile rotamer that minimized steric clashes with the surrounding residues. We added crystallographic waters, resolved in the 1GZM dark state structure. Cysteines 322 and 323 were palmitoylated. Glu, Asp, Arg, and Lys residues were set as charged, except E122$^{3.37}$ and D83$^{2.50}$ [40]. We also set up additional models where E113$^{3.28}$ was considered neutral. Topology and parameter definitions for palmitoyl-cysteine and retinal bound via protonated Schiff base link to lysine were obtained from the parameter/topology repository of NAMD.

The models of WT(c-c) and mutant rhodopsin were embedded in a solvated and pre-equilibrated lipid bilayer consisting of ~300 molecules of 1-palmitoyl-2-oleoyl-sn-glycerol-3-phosphatidylcholine (POPC) and ~22,000 water molecules. Sodium and chloride ions were added to a concentration of 0.15 M NaCl, and then additional ions were added to achieve charge neutrality. The system measured roughly 75 × 75 × 90 Å^3, with a total of ~59,000 atoms. These systems were equilibrated as follows: First, a short (0.5 ns) simulation was performed in which only the lipid tails were allowed to move, in order to induce the appropriate disorder of a fluid-like bilayer. Then, the geometry of the entire system was optimized by 1,000 steps of energy minimization, followed by two equilibration steps with the protein constrained (0.5 ns) and without constraints (0.5 ns). In order to estimate the structural stability of the retinal binding site, the equilibrated structures were subjected to 15 ns of simulated annealing, where the temperature was raised from 300 K to 450 K in 7.5 ns and then lowered to 300 K in 7.5 ns. Simulations were carried out using NAMD 2.8 [49,50] at constant pressure (1 atm), and using a time step of 2 fs.

Data availability

Coordinates and structure factors have been deposited under pdb code 5EN0 for T94I/GaCT2 and 5DYS for T94I.

Expanded View for this article is available online.

Acknowledgements
We are very grateful for the large-scale expression of rhodopsin mutations done by Georg Schmid and Roger Dawson from the Pharma Research and Early Development at the Roche Innovation Center Basel. We thank the team from the Macromolecular crystallography group at the Swiss Light Source (SLS) for support during data collection. The work was financially supported by the Swiss National Science Foundation grants SNF 31003A_141235 (to J.S.), SNF 31003A_159558 (to J.S.) and SNF 310030_153145 (to G.S.).

Author contributions
AS prepared stable cell lines, purified, and crystallized mutated rhodopsin. AS and JS collected X-ray diffraction data and solved the structures. YG and ECYY contributed the experiments characterizing the rhodopsin decay rates. MM and XD did molecular dynamic simulations to characterize the impact of mutations on the rhodopsin dark state. GS contributed to planning and initiated contact between participating research groups. XD, ECYY, and JS supervised the project and analyzed data. AS, XD, and JS wrote the paper with additions and critical comments from all authors.

Conflict of interest
The authors declare that they have no conflict of interest.

References

1. Smit MJ, Vischer HF, Bakker RA, Jongejan A, Timmerman H, Pardo L, Leurs R (2007) Pharmacogenomic and structural analysis of constitutive g protein-coupled receptor activity. *Annu Rev Pharmacol Toxicol* 47: 53 – 87
2. Baylor DA, Nunn BJ, Schnapf JL (1987) Spectral sensitivity of cones of the monkey *Macaca fascicularis*. *J Physiol* 390: 145 – 160
3. Melia TJ, Cowan CW, Angleson JK, Wensel TG (1997) A comparison of the efficiency of G protein activation by ligand-free and light-activated forms of rhodopsin. *Biophys J* 73: 3182 – 3191
4. Park PS-H (2014) Constitutively active rhodopsin and retinal disease. *Adv Pharmacol* 70: 1 – 36
5. Robinson PRP, Cohen GBG, Zhukovsky EAE, Oprian DDD (1992) Constitutively active mutants of rhodopsin. *Neuron* 9: 719 – 725
6. Rim JJ, Oprian DDD (1995) Constitutive activation of opsin: interaction of mutants with rhodopsin kinase and arrestin. *Biochemistry* 34: 11938 – 11945
7. Rao VR, Cohen GB, Oprian DD (1994) Rhodopsin mutation G90D and a molecular mechanism for congenital night blindness. *Nature* 367: 639 – 642
8. Gross AK, Rao VR, Oprian DD (2003) Characterization of rhodopsin congenital night blindness mutant T94I. *Biochemistry* 42: 2009 – 2015
9. Sieving PA, Richards JE, Naarendorp F, Bingham EL, Scott K, Alpern M (1995) Dark-light: model for nightblindness from the human rhodopsin Gly-90–>Asp mutation. *Proc Natl Acad Sci USA* 92: 880 – 884
10. Zeitz C, Gross AK, Leifert D, Kloeckener-Gruissem B, McAlear SD, Lemke J, Neidhardt J, Berger W (2008) Identification and functional characterization of a novel rhodopsin mutation associated with autosomal dominant CSNB. *Invest Ophthalmol Vis Sci* 49: 4105 – 4114
11. al-Jandal N, Farrar GJ, Kiang AS, Humphries MM, Bannon N, Findlay JB, Humphries P, Kenna PF (1999) A novel mutation within the rhodopsin gene (Thr-94-Ile) causing autosomal dominant congenital stationary night blindness. *Hum Mutat* 13: 75 – 81

12. McAlear SD, Kraft TW, Gross AK (2010) 1 rhodopsin mutations in congenital night blindness. *Adv Exp Med Biol* 664: 263 – 272
13. Sieving PA, Fowler ML, Bush RA, Machida S, Calvert PD, Green DG, Makino CL, McHenry CL (2001) Constitutive "light" adaptation in rods from G90D rhodopsin: a mechanism for human congenital nightblindness without rod cell loss. *J Neurosci* 21: 5449 – 5460
14. Dizhoor AM, Woodruff ML, Olshevskaya EV, Cilluffo MC, Cornwall MC, Sieving PA, Fain GL (2008) Night blindness and the mechanism of constitutive signaling of mutant G90D rhodopsin. *J Neurosci* 28: 11662 – 11672
15. Naash MI, Wu T-H, Chakraborty D, Fliesler SJ, Ding X-Q, Nour M, Peachey NS, Lem J, Qtaishat N, Al-Ubaidi MR *et al* (2004) Retinal abnormalities associated with the G90D mutation in opsin. *J Comp Neurol* 478: 149 – 163
16. Singhal A, Ostermaier MK, Vishnivetskiy SA, Panneels V, Homan KT, Tesmer JJG, Veprintsev D, Deupi X, Gurevich VV, Schertler GFX *et al* (2013) Insights into congenital stationary night blindness based on the structure of G90D rhodopsin. *EMBO Rep* 14: 520 – 526
17. Choe H-W, Kim YJ, Park JH, Morizumi T, Pai EF, Krauss N, Hofmann KP, Scheerer P, Ernst OP (2011) Crystal structure of metarhodopsin II. *Nature* 471: 651 – 655
18. Xie G, Gross AK, Oprian DD (2003) An opsin mutant with increased thermal stability. *Biochemistry* 42: 1995 – 2001
19. Standfuss J, Xie G, Edwards PC, Burghammer M, Oprian DD, Schertler GFX (2007) Crystal structure of a thermally stable rhodopsin mutant. *J Mol Biol* 372: 1179 – 1188
20. Standfuss J, Zaitseva E, Mahalingam M, Vogel R (2008) Structural impact of the E113Q counterion mutation on the activation and deactivation pathways of the G protein-coupled receptor rhodopsin. *J Mol Biol* 380: 145 – 157
21. Deupi X, Edwards P, Singhal A, Nickle B, Oprian D, Schertler G, Standfuss J (2012) Stabilized G protein binding site in the structure of constitutively active metarhodopsin-II. *Proc Natl Acad Sci USA* 109: 119 – 124
22. Cooper A, Dixon SF, Nutley MA (1987) Mechanism of retinal Schiff base formation and hydrolysis in relation to visual pigment photolysis and regeneration: resonance Raman spectroscopy of a tetrahedral carbinolamine intermediate and oxygen-18 labeling of retinal at the metarhodopsin stage in photoreceptor membranes. *J Am Chem Soc* 109: 7254 – 7263
23. Guo Y, Sekharan S, Liu J, Batista VS, Tully JC, Yan ECY (2014) Unusual kinetics of thermal decay of dim-light photoreceptors in vertebrate vision. *Proc Natl Acad Sci USA* 111: 10438 – 10443
24. Janz JM, Farrens DL (2004) Role of the retinal hydrogen bond network in rhodopsin Schiff base stability and hydrolysis. *J Biol Chem* 279: 55886 – 55894
25. Liu J, Liu MY, Nguyen JB, Bhagat A, Mooney V, Yan ECY (2009) Thermal decay of rhodopsin: role of hydrogen bonds in thermal isomerization of 11-cis retinal in the binding site and hydrolysis of protonated Schiff base. *J Am Chem Soc* 131: 8750 – 8751
26. Piechnick R, Ritter E, Hildebrand PW, Ernst OP, Scheerer P, Hofmann KP, Heck M (2012) Effect of channel mutations on the uptake and release of the retinal ligand in opsin. *Proc Natl Acad Sci USA* 109: 5247 – 5252
27. Liu J, Liu MY, Fu L, Zhu GA, Yan ECY (2011) Chemical kinetic analysis of thermal decay of rhodopsin reveals unusual energetics of thermal isomerization and hydrolysis of Schiff base. *J Biol Chem* 286: 38408 – 38416
28. Liu J, Liu MY, Nguyen JB, Bhagat A, Mooney V, Yan ECY (2011) Thermal properties of rhodopsin: insight into the molecular mechanism of dim-light vision. *J Biol Chem* 286: 27622 – 27629
29. Toledo D, Ramon E, Aguilà M, Cordomí A, Pérez JJ, Mendes HF, Cheetham ME, Garriga P (2011) Molecular mechanisms of disease for mutations at Gly-90 in rhodopsin. *J Biol Chem* 286: 39993 – 40001
30. Kim J-M, Altenbach C, Kono M, Oprian DD, Hubbell WL, Khorana HG (2004) Structural origins of constitutive activation in rhodopsin: role of the K296/E113 salt bridge. *Proc Natl Acad Sci USA* 101: 12508 – 12513
31. Kawamura S, Colozo AT, Ge L, Muller DJ, Park PS-H (2012) Structural, energetic, and mechanical perturbations in a rhodopsin mutant that causes congenital stationary night blindness. *J Biol Chem* 26: 21826 – 21835
32. Zhukovsky EA, Oprian DD (1989) Effect of carboxylic acid side chains on the absorption maximum of visual pigments. *Science* 246: 928 – 930
33. Sakmar TP, Franke RR, Khorana HG (1989) Glutamic acid-113 serves as the retinylidene Schiff base counterion in bovine rhodopsin. *Proc Natl Acad Sci USA* 86: 8309 – 8313
34. Fahmy K, Zvyaga TA, Sakmar TP, Siebert F (1996) Spectroscopic evidence for altered chromophore–protein interactions in low-temperature photoproducts of the visual pigment responsible for congenital night blindness. *Biochemistry* 35: 15065 – 15073
35. Ramon E, del Valle LJ, Garriga P (2003) Unusual thermal and conformational properties of the rhodopsin congenital night blindness mutant Thr-94 –> Ile. *J Biol Chem* 278: 6427 – 6432
36. Zvyaga TA, Fahmy K, Siebert F, Sakmar TP (1996) Characterization of the mutant visual pigment responsible for congenital night blindness: a biochemical and Fourier-transform infrared spectroscopy study. *Biochemistry* 35: 7536 – 7545
37. Vogel R, Siebert F (2001) Conformations of the active and inactive states of opsin. *J Biol Chem* 276: 38487 – 38493
38. Vishnivetskiy SA, Ostermaier MK, Singhal A, Panneels V, Homan KT, Glukhova A, Sligar SG, Tesmer JJG, Schertler GFX, Standfuss J *et al* (2013) Constitutively active rhodopsin mutants causing night blindness are effectively phosphorylated by GRKs but differ in arrestin-1 binding. *Cell Signal* 25: 2155 – 2162
39. Jin S, Cornwall MC, Oprian DD (2003) Opsin activation as a cause of congenital night blindness. *Nat Neurosci* 6: 731 – 735
40. Mahalingam M, Martínez-Mayorga K, Brown MF, Vogel R (2008) Two protonation switches control rhodopsin activation in membranes. *Proc Natl Acad Sci USA* 105: 17795 – 17800
41. Mattle D, Singhal A, Schmid G, Dawson R, Standfuss J (2014) Mammalian expression, purification, and crystallization of rhodopsin variants. *Methods Mol Biol* 1271: 39 – 54
42. Kabsch W (2010) Xds. *Acta Crystallogr D Biol Crystallogr* 66: 125 – 132
43. McCoy AJ, Grosse-Kunstleve RW, Adams PD, Winn MD, Storoni LC, Read RJ (2007) Phaser crystallographic software. *J Appl Crystallogr* 40: 658 – 674
44. Emsley P, Cowtan K (2004) Coot: model-building tools for molecular graphics. *Acta Crystallogr D Biol Crystallogr* 60: 2126 – 2132
45. Adams PD, Grosse-Kunstleve RW, Hung LW, Ioerger TR, McCoy AJ, Moriarty NW, Read RJ, Sacchettini JC, Sauter NK, Terwilliger TC (2002) PHENIX: building new software for automated crystallographic structure determination. *Acta Crystallogr D Biol Crystallogr* 58: 1948 – 1954

46. Alexandrov AI, Mileni M, Chien EYT, Hanson MA, Stevens RC (2008) Microscale fluorescent thermal stability assay for membrane proteins. *Structure* 16: 351 – 359
47. Liu MY, Liu J, Mehrotra D, Liu Y, Guo Y, Baldera-Aguayo PA, Mooney VL, Nour AM, Yan ECY (2013) Thermal stability of rhodopsin and progression of retinitis pigmentosa: a comparison of S186W and D190N rhodopsin mutants. *J Biol Chem* 24: 17698 – 176712
48. Li J, Edwards PC, Burghammer M, Villa C, Schertler GFX (2004) Structure of bovine rhodopsin in a trigonal crystal form. *J Mol Biol* 343: 1409 – 1438
49. Phillips JC, Braun R, Wang W, Gumbart J, Tajkhorshid E, Villa E, Chipot C, Skeel RD, Kalé L, Schulten K (2005) Scalable molecular dynamics with NAMD. *J Comput Chem* 26: 1781 – 1802
50. MacKerell AD, Bashford D, Bellott M (1998) All-atom empirical potential for molecular modeling and dynamics studies of proteins. *J Phys Chem B* 102: 3586 – 3616

